Synthesis and Characterization of Functionalized Mesoporous Silica by Aerosol-Assisted Self-Assembly

Xiangling Ji,[†,§] Qingyuan Hu,[†] J. Eric Hampsey,[†] Xuepeng Qiu,[§] Lianxun Gao,[§] Jibao He,[‡] and Yunfeng Lu*[,†]

Department of Chemical and Biomolecular Engineering and Central Instrumental Facilities, Tulane University, New Orleans, Louisiana 70118, and Polymer Engineering Laboratory, Changchun Institute of Applied Chemistry, Chinese Academy of Sciences, Changchun 130022, China

Received December 14, 2005. Revised Manuscript Received February 3, 2006

An efficient, productive, and low-cost aerosol-assisted self-assembly process has been developed to produce organically modified mesoporous silica particles via a direct co-condensation of silicate species and organosilicates that contain nonhydrolyzable functional groups in the presence of templating surfactant molecules. Different surfactants including cetyltrimethylammonium bromide, nonionic surfactant Brij-56, and triblock copolymer P123 have been used as the structure-directing agents. The organosilanes used in this study include tridecafluoro-1,1,2,2-tetrahydrooctyltriethoxysilane, methytriethoxysilane, vinyltrimethoxysilane, and 3-(trimethoxysilyl)propyl methacrylate. X-ray diffraction and transmission electron microscopy studies indicate the formation of particles with various mesostructures. Fourier transform infrared and solid-state nuclear magnetic resonance spectra confirm the organic ligands are covalently bound to the surface of the silica framework. The porosity, pore size, and surface area of the particles were characterized using nitrogen adsorption and desorption measurements. This method provides a direct synthesis route to efficiently synthesize a large variety of organic functionalized mesoporous silica particles with controlled pore sizes, pore surface chemistry, and pore structures for catalyst, filler, and other applications.

Introduction

Since the first report of MCM-41 with ordered hexagonal arrays of pore channels in the early 1990s,[1] this field has attracted much interest due to its potential applications in catalysts, membrane separation and sensors, electronics, and other areas.[2−5] Considerable attention has been focused on tailoring the chemical composition of mesoporous materials for applications in catalysis and fabrication of nanocomposites. Therefore, surface modification plays an important role in mesoporous silica materials. Tailoring of these materials for specific applications requires both structural and compositional control. This can be achieved by chemical modification through postsynthesis activation of the mesostructured product or via direct synthesis.[6−25]

Mesoporous silica possesses many silanol (SiOH) groups on the surface that can act as convenient anchoring points for organic functionalization. A postsynthesis process has been widely employed to anchor specific organic groups onto the surface of silanols of diversely prefabricated silica supports.[6−11] Typically, organochlorosilanes or organoalkoxysilanes are used as precursors for the surface modification. Other than the above-mentioned organosilane, a number of silane-coupling agents, such as olefins, nitriles, alkanethiols, epoxides, and other surface groups, are also employed to

* To whom correspondence should be addressed. Phone: (504) 865-5827. Fax: (504) 865-6744. E-mail: ylu@tulane.edu.
[†] Department of Chemical and Biomolecular Engineering, Tulane University.
[‡] Central Instrumental Facilities, Tulane University.
[§] Chinese Academy of Sciences.

(1) Kresge, C. T.; Leonowicz, M. E.; Roth, W. J.; Vartuli, J. C.; Beck, J. S. *Nature* **1992**, *359*, 710.
(2) Dams, M.; Drijkoningen, L.; Pauwels, B.; Van, T. G.; De Vos, D. E.; Jacobs, P. A. *J. Catal.* **2002**, *209*, 225.
(3) Hu, Q.; Pang, J.; Jiang, N.; Hampsey, J. E.; Lu, Y. *Microporous Mesoporous Mater.* **2005**, *81*, 149.
(4) Pang, J.; Hampsey, J. E.; Wu, Z.; Hu, Q.; Lu, Y. *Appl. Phys. Lett.* **2004**, *85*, 4889.
(5) Tanaka, S.; Mizukami, F.; Niwa, S.; Toba, M.; Maeda, K.; Shimada, H.; Kunimori, K. *Appl. Catal., A* **2002**, *229*, 165.
(6) Lindlar, B.; Luechinger, M.; Roethlisberger, A.; Haouas, M.; Pirngruber, G.; Kogelbauer, A.; Prins, R. *J. Mater. Chem.* **2002**, *12*, 528.
(7) Feng, X.; Fryxell, G. E.; Wang, L. Q.; Kim, A. Y.; Liu, J.; Kemner, K. M. *Science* **1997**, *276*, 923.
(8) Vinu, A.; Hossain, K. Z.; Ariga, K. *J. Nanosci. Nanotechnol.* **2005**, *5*, 347.
(9) Zhang, W. H.; Lu, X. B.; Xiu, J. H.; Hua, Z. L.; Zhang, L. X.; Robertson, M.; Shi, J. L.; Yan, D. S.; Holmes, J. D. *Adv. Funct. Mater.* **2004**, *14*, 544.
(10) Yokoi, T.; Yoshitake, H.; Tatsumi, T. *J. Mater. Chem.* **2004**, *14*, 951.
(11) Stein, A.; Melde, B. J.; Schroden, R. C. *Adv. Mater.* **2000**, *12*, 1403.
(12) Burkett, S. L.; Sims, S. D.; Mann, S. *Chem. Commun.* **1996**, *11*, 1367.
(13) Lim, M. H.; Stein, A. *Chem. Mater.* **1999**, *11*, 3285.
(14) Lim, M. H.; Blanford, C. F.; Stein, A. *J. Am. Chem. Soc.* **1997**, *119*, 4090.
(15) Fowler, C. E.; Burkett, S. L.; Mann, S. *Chem. Commun.* **1997**, 1769.
(16) Hu, Q.; Jiang, N.; Hampsey, J. E.; Li, C. J.; Lu, Y. *Chem. Mater.* **2005**, *17*, 1561.
(17) Fowler, C. E.; Lebeau, B.; Mann, S. *Chem. Commun.* **1998**, 1825.
(18) Bambrough, C. M.; Slade, R. C. T.; Williams, R. T. *J. Mater. Chem.* **1998**, *8*, 569.
(19) Lim, M. H.; Blanford, C. F.; Stein, A. *Chem. Mater.* **1998**, *10*, 467.
(20) Babonneau, F.; Leite, L.; Fontlupt, S. *J. Mater. Chem.* **1999**, *9*, 175.
(21) Richer, R.; Mercier, L. *Chem. Commun.* **1998**, 1775.
(22) Shimojima, A.; Kuroda, K. *Langmuir* **2002**, *18*, 1144.
(23) Wang, Y.; Zibrowius, B.; Yang, C.; Spliethoff, B.; Schueth, F. *Chem. Commun.* **2004**, 46.
(24) Wang, Y. Q.; Yang, C. M.; Zibrowius, B.; Spliethoff, B.; Linden, M.; Schueth, F. *Chem. Mater.* **2003**, *15*, 5029.
(25) Ganschow, M.; Wark, M.; Wohrle, D.; Schulz-Ekloff G. *Angew. Chem., Int. Ed.* **2000**, *39*, 161.

10.1021/cm052764p CCC: $33.50
Published on Web 03/29/2006

functionalize the surface of mesoporous silica.[11] Control over the concentration and distribution of organic moieties in MCM-41 by postsynthesis is constrained by the number of surface silanol groups and by their accessibility. The grafting rates depend on the reactivity of the precursors, diffusion limitations, and steric factors.

The direct-synthesis approach involves co-condensation of silicate species and organosilicates that contain nonhydrolyzable functional ligands in the presence of templating surfactant molecules. This approach has led to many organic-group-functionalized mesoporous silica materials with various surface functional groups, such as phenyl, *n*-octyl, thiol, amine, epoxide, imidazole, or allyl.[12−25] The first organically modified mesoporous silica material prepared by direct synthesis was reported in 1996.[12] This single-step synthesis can produce mesoporous solids with high loadings of organic functional groups and homogeneous surface coverage within a relatively short preparation time.[13] A bromination reaction of vinyl-functionalized MCM-41 provides evidence for attachment of most vinyl groups to the accessible surface within the mesopore channels.[14]

A variety of strategies have been proposed to synthesize mesoporous materials. A commonly used organic/inorganic nanocomposite synthesis process involves the simultaneous coassembly of surfactants and other building blocks such as inorganic silicate species. Among these methods, aerosol-assisted self-assembly using a surfactant or block copolymer as the template is shown as one of the powerful methods for synthesizing ordered mesoporous particles and thin films.[26−38] The synthesis process starts with homogeneous ethanol/water solutions containing soluble silicate and surfactant. Using the apparatus depicted in Figure 1, aerosol droplets generated from the atomizer are subsequently dried in the drying zone, heated in the heating zone, and collected in the filter. Solvent evaporation during this process enriches nonvolatile components and induces their coassembly confined within the aerosol droplets into ordered liquid-crystalline mesophases.[39,40] To date, this process can be widely used to prepare various mesoporous materials including mesoporous silica and carbon with precise control of the mesostructure and morphology. Mesoporous silica particles that exhibit surface areas greater than 1200 m^2/g, controllable pore sizes in the range of 2−20 nm, controlled pore surface chemistry, and controlled pore channels (e.g., hexagonal, cubic, lamellar, vesicular, ordered core/shell structure, or disordered pore channels) have been fabricated through manipulation of the cooperative assembly of surfactants and silicates. Monodisperse mesoporous silica microspheres are formed by a vibrating orifice aerosol generator (VOAG).[36] Here, we extend this simple one-pot synthesis to mesoporous silica aerosol particles functionalized with fluoro, methyl, vinyl, and methacrylate groups through template-directed co-condensation of tetraethyl orthosilicate (TEOS) and organotrialkoxysilanes ($(OR)_3SiR'$) under acidic conditions. This process presents an economically feasible production of modified mesoporous silica particles for future catalyst, filler, and other applications.

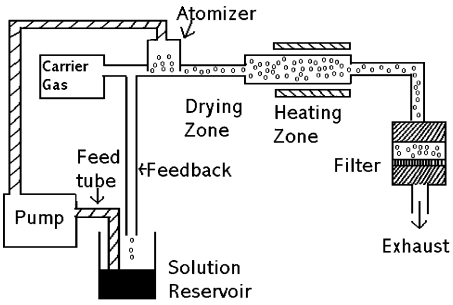

Figure 1. Diagram of the aerosol reactor.

Table 1. Starting Composition of Sols

sample no.	molar ratio[a]	sample no.	molar ratio[a]
F1	TEOS:TFTS = 90:10	V2	TEOS:VTMS = 86:14
M1	TEOS:MTES = 78:22	V3	TEOS:VTMS = 93:7
V1	TEOS:VTMS = 73:27	T1	TEOS:TMSPMA = 70:30

[a] TEOS = tetraethyl orthosilicate, TFTS = tridecafluoro-1,1,2,2-tetrahydrooctyltriethoxysilane, MTES = methyltriethoxysilane, VTMS = vinyltrimethoxysilane, and TMSPMA = 3-(trimethoxysilyl)propyl methacrylate.

Experimental Section

Preparation of Functionalized Mesoporous Silica Particles. A typical formulation is as follows: 4 mL of TEOS, 1 mL of functionalized organosilane (TFTS = tridecafluoro-1,1,2,2-tetrahydrooctyltriethoxysilane, MTES = methyltriethoxysilane, VTMS = vinyltrimethoxysilane, TMSPMA = 3-(trimethoxysilyl)propyl methacrylate), surfactant (1.25 g of CTAB ($CH_3(CH_2)_{15}N^+(CH_3)_3Br^-$), 2 g of Brij-56 ($CH_3(CH_2)_{15}(OCH_2CH_2)_{10}OH$), or 2 g of P123 (($CH_2$-$CH_2O)_{20}(CH_2(CH_3)CH_2O)_{70}(CH_2CH_2O)_{20}$)), 2 g of 0.1 N HCl, and 50 mL of ethanol. The starting composition is listed in Table 1. The blank silica samples without any modifying agents were prepared at the same conditions as a reference.[26]

Surface treatment and removal of the surfactant were carried out by adding 1.2 mL of HMDS (1,1,1,3,3,3-hexamethyldisilazane) and 4.8 mL of ethanol to the methyl-, vinyl-, or methacrylate-modified particles, placing the mixture in an ultrasonicator for 30 min, centrifuging, and finally rinsing with 10 mL of ethanol for three

(26) Lu, Y.; Fan, H.; Stump, A.; Ward, T. L.; Rieker, T.; Brinker, C. J. *Nature* **1999**, *398*, 223.
(27) Baccile, N.; Grosso, D.; Sanchez, C. *J. Mater. Chem.* **2003**, *13*, 3011.
(28) Kim, S. H.; Liu, B. Y. H.; Zachariah, M. R. *Langmuir* **2004**, *20*, 2523.
(29) Bore, M. T.; Rathod, S. B.; Ward, T. L.; Datye, A. K. *Langmuir* **2003**, *19*, 256.
(30) Areva, S.; Boissiere, C.; Grosso, D.; Asakawa, T.; Sanchez, C.; Linden, M. *Chem. Commun.* **2004**, 1630.
(31) Lu, Y.; McCaughey, B. F.; Wang, D.; Hampsey, J. E.; Doke, N.; Yang, Z.; Brinker, C. J. *Adv. Mater.* **2003**, *15*, 1733.
(32) Xomeritakis, G.; Braunbarth, C. M.; Smarsly, B.; Liu, N.; Kohn, R.; Klipowicz, Z.; Brinker, C. J. *Microporous Mesoporous Mater.* **2003**, *66*, 91.
(33) Buranda, T.; Huang, J.; Ramarao, G. V.; Ista, L. K.; Larson, R. S.; Ward, T. L.; Sklar, L. A.; Lopez, G. P. *Langmuir* **2003**, *19*, 1654.
(34) Rao, G. V. R.; Lopez, G. P.; Bravo, J.; Pham, H.; Datye, A. K.; Xu, H.; Ward, T. L. *Adv. Mater.* **2002**, *14*, 1301.
(35) Hampsey, J. E.; Arsenault, S.; Hu, Q.; Lu, Y. *Chem. Mater.* **2005**, *17*, 2475.
(36) Bore, M. T.; Ward, T. L.; Fukuoka, A.; Datye, A. K. *Catal. Lett.* **2004**, *98*, 167.
(37) Hampsey, J. E.; Hu, Q.; Rice, L.; Pang, J.; Wu, Z.; Lu, Y. *Chem. Comm.* **2005**, 3606.
(38) Hampsey, J. E.; Hu, Q.; Wu, Z.; Rice, L.; Pang, J.; Lu, Y. *Carbon* **2005**, *43*, 2977.
(39) Lu, Y.; Ganguli, R.; Drewien, C. A.; Anderson, M. T.; Brinker, C. J.; Gong, W.; Guo, Y.; Soyez, H.; Dunn, B.; Huang, M. H.; Zink, J. I. *Nature* **1997**, *389*, 364.
(40) Nishida, F.; McKiernan, J. M.; Dunn, B.; Zink, J. I.; Brinker, C. J.; Hurd, A. J. *J. Am. Ceram. Soc.* **1995**, *78*, 1640.

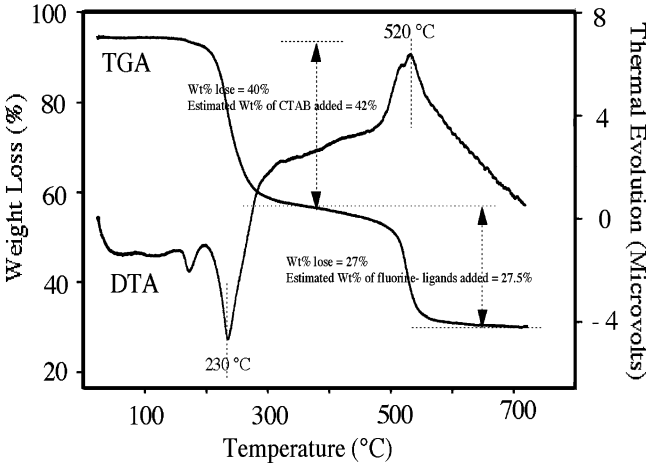

Figure 2. TGA/DTA curves of the TFTS/TEOS (15:85) hybrid particles using a nitrogen atmosphere and a heating rate of 4 °C/min.

cycles. The samples were then dried in a vacuum oven. The surfactant was removed from the TFTS-modified particles by heating at 350 °C under nitrogen for 5 h. This approach is based on heating the surfactant/hybrid materials in an inert atmosphere using heating temperatures that are high enough to decompose the surfactants without degrading the covalently bound organic ligands.

Characterization. Thermogravimetric analysis/differential thermal analysis (TGA/DTA) experiments were performed using a Polymer Labs STA 1500 instrument using air, oxygen, or argon as the processing atmosphere and a heating rate of 4 °C/min. X-ray powder diffraction (XRD) data were acquired on a Scintag XDS 2000 X-ray diffractometer equipped with monochromated Cu Kα radiation ($\lambda = 1.5406$ Å). Typically, the data were collected in the range of $0.8° < 2\theta < 6°$ with a step size of 0.01° and a count time of 1 s per step. Transmission electron microscopy (TEM) images were taken with a JEOL 2010 electron microscope with an accelerating voltage of 120 kV. The samples were prepared by dispersing the silica particles directly on copper grids. Infrared spectra of the samples were recorded on a NEXUS 670 FT-IR spectrometer (Thermo Nicolet Co.) with a resolution of 4 cm^{-1}. The samples were prepared with a conventional KBr pressing method. Both solid-state ^{13}C and ^{29}Si magic-angle spinning (MAS) NMR experiments were performed at room temperature on a 400 MHz AV400 NMR spectrometer (Bruker, Switzerland). Nitrogen adsorption−desorption isotherms at 77 K for mesoporous silica particles were obtained using a Micromeritics ASAP 2010. The specific surface area was calculated by the Brunauer−Emmett−Teller (BET) method, while the pore size was obtained from the Barrett−Joyner−Halenda (BJH) model. The samples posttreated with HMDS were degassed for 6 h at 200 °C, while the other samples were degassed for 6 h at 100 °C.

Results and Discussion

Thermal Analysis. Figure 2 shows TGA/DTA curves of the TFTS/TEOS (mole ratio 15:85) hybrid particles using a nitrogen atmosphere and a heating rate of 4 °C/min. The first step of weight loss (∼40%) accompanied by the endothermic peaks at 170 and 230 °C is due to the decomposition of CTAB in nitrogen (the melting and decomposition temperatures for CTAB are around 230 °C). This weight loss corresponds to that of CTAB added in the hybrid particles (∼40%). The second step of weight loss (∼27%) accompanied by an exothermic peak at 520 °C corresponds to the decomposition of tridecafluoro-1,1,2,2-tetrahydrooctyl ligands; the measured weight loss is consistent with that of tridecafluoro-1,1,2,2-tetrahydrooctyl ligands added (∼28%). No significant weight loss and heat release are observed at temperatures between 300 and 450 °C. Thus, the CTAB-containing hybrid materials can be heated to 350 °C in a nitrogen atmosphere to selectively remove the CTAB but not the fluorinated organic ligands.

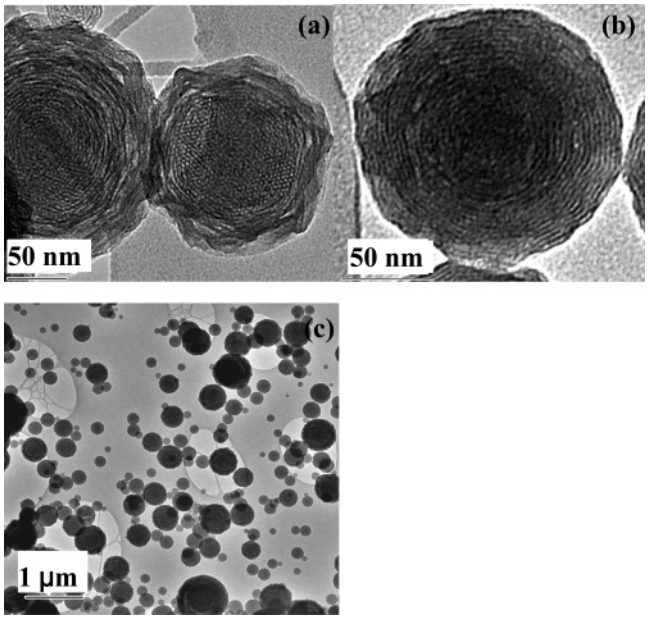

Figure 3. TEM images of 6% CTAB TFTS-modified silica particles: (a) before removal of surfactant, (b) after removal of surfactant, and (c) highly dispersed on the TEM grid showing hydrophobicity.

Powder X-ray diffraction and Transmission Electron Microscopy. *(a) Fluoro Functionalization.* Figure 3a shows a TEM image of the 6% CTAB TFTS-modified silica particles before calcination. It clearly shows the formation of a silica/TFTS vesicular structure with surface dimples. Figure 3b shows a TEM image of silica/TFTS hybrid particles after selective removal of the CTAB. It clearly demonstrates the partial transformation of the original vesicular structure to a hexagonal structure upon calcination. We believe this transformation is driven by the high curvature of the vesicle interior. Usually, silica/CTAB tends to form hexagonal mesophase particles during the aerosol process.[26] However, the addition of TFTS results in a vesicular structure, which is probably due to coassembly of hydrolyzed TFTS molecules along with CTAB. TFTS becomes an amphiphilic molecule upon hydrolysis and serves as a cosurfactant, leading to the formation of the vesicular structure. Another possible explanation is the incorporation of TFTS may retard the phase transformation from the vesicular to the hexagonal structure. Further experiments are needed to understand this issue.

Hydrolyzed TFTS serves as a cosurfactant, is incorporated into the micelles, and imparts hydrophobicity to the particles, resulting in the formation of highly dispersed particles, which may be important to prepare highly dispersed fillers for composite materials. This is confirmed by the TEM results shown in Figure 3c.

(b) Post-treatment with HMDS. Figures 4 and 5, respectively, show the XRD patterns and TEM images of the

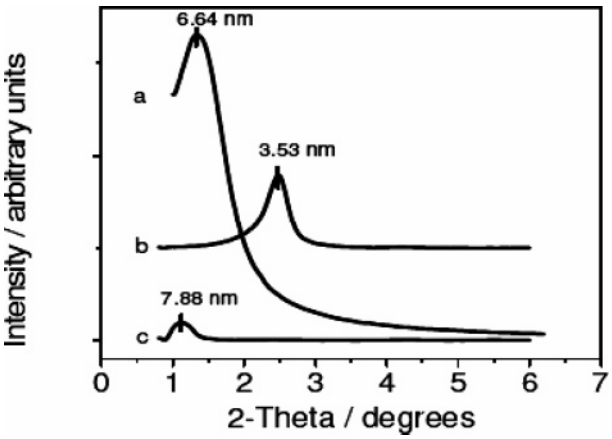

Figure 4. XRD patterns for the silica particles posttreated with HMDS: (a) Brij-56, (b) CTAB, and (c) P123 as the template.

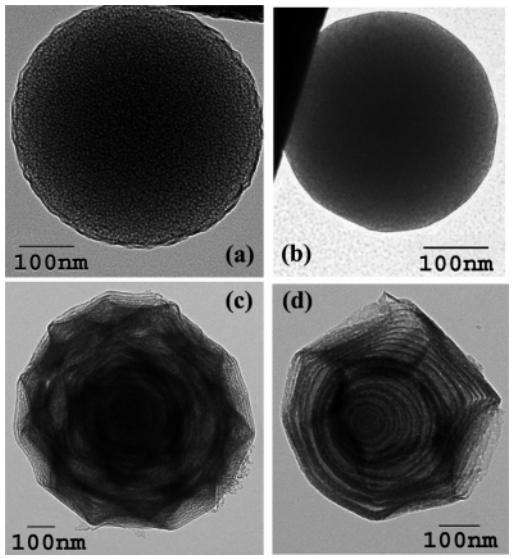

Figure 5. TEM images for the silica particles posttreated with HMDS: (a) Brij-56, (b) CTAB, and (c, d) P123 as the template.

mesostructured particles posttreated with HMDS. The Brij-56-templated particles show a wormlike pore structure in Figure 5a with a center-to-center distance of 6.67 nm, while their XRD pattern shown in Figure 4a consistently shows a diffraction peak at a 2θ of 1.33°, which corresponds to a d spacing of 6.64 nm. The particles synthesized with CTAB display a hexagonal structure in Figure 5b with a center-to-center distance around 3.60 nm, which matches an intense (100) diffraction peak at a 2θ of 2.50°, which corresponds to a d_{100} spacing of 3.53 nm, shown in Figure 4b. The XRD pattern of the P123-templated particles displayed in Figure 4c shows a diffraction peak at a 2θ of 1.12°, which corresponds to a d spacing of 7.88 nm. The TEM images in Figure 5c,d indicate that the P123 particles exhibit a lamellar-like mesostructure. Note the dimpling morphology shown in Figure 5c, which is caused by shrinkage of the particle during the drying process.

(c) Methyl Functionalization. Figures 6 and 7 show the XRD patterns and TEM images obtained from methyl-functionalized silica aerosol particles. In Figure 6a, the Brij-56-templated particles show a diffraction peak at a 2θ of 1.39°, which corresponds to a d spacing of 6.35 nm, which is similar to the center-to-center distance of 6.40 nm of the

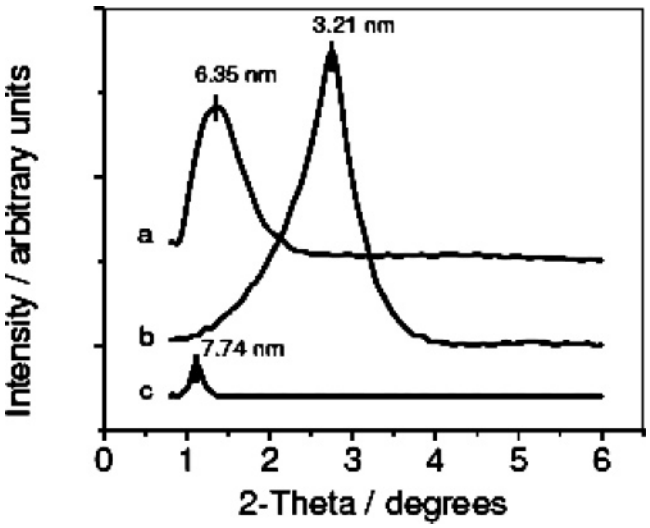

Figure 6. XRD patterns for methyl-modified particles: (a) Brij-56, (b) CTAB, and (c) P123 as the template.

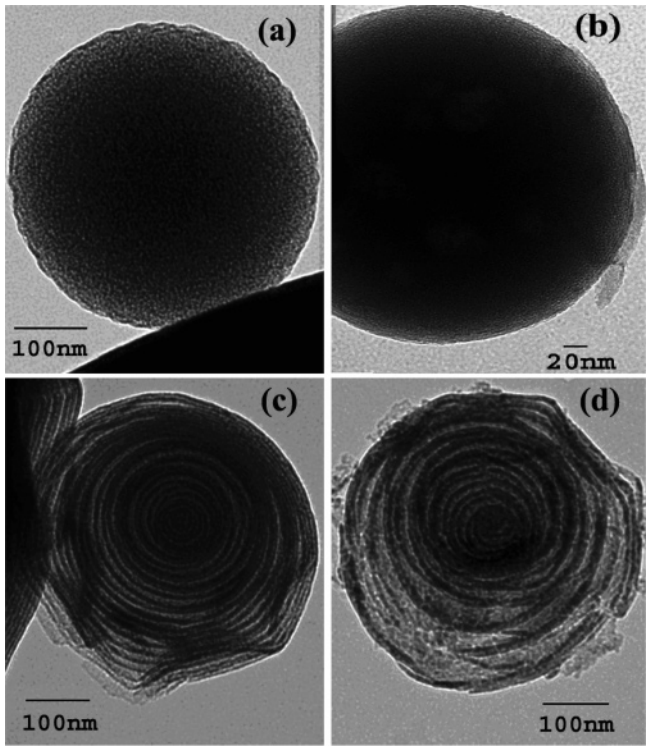

Figure 7. TEM images for methyl-modified silica particles: (a) Brij-56, (b) CTAB, and (c, d) P123 as the template.

wormlike pores observed in Figure 7a. A single XRD peak at a 2θ of 2.75°, which corresponds to a d spacing of 3.21 nm, is observed in Figure 6b for particles with CTAB as the structure-directing agent, while local ordered pore arrays can be found in the TEM image in Figure 7b. The P123-templated particles exhibit a diffraction peak at a 2θ of 1.14°, which corresponds to a d_{100} spacing of approximately 7.74 nm, and their TEM images shown in Figure 7c,d show a lamellar mesostrucuture. Compared to the particles post-treated with HMDS, methyl-modified samples possess a decreased d spacing of the first diffraction peak due to an attachment of methyl groups to the internal surfaces of the pores, resulting in a decreased pore size.

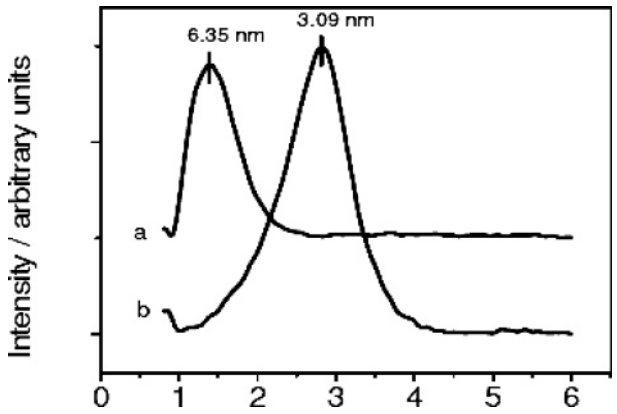

Figure 8. XRD patterns for vinyl-modified particles: (a) Brij-56 and (b) CTAB as the template.

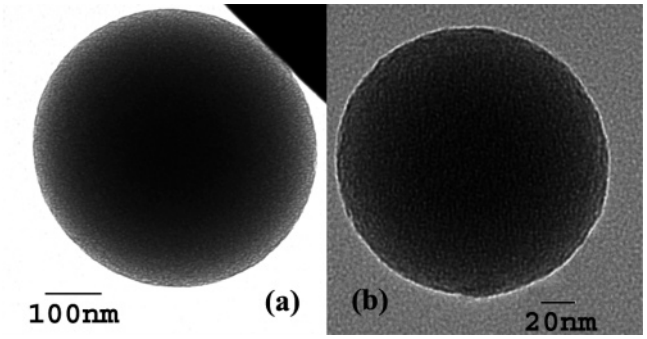

Figure 9. TEM images for vinyl-modified silica particles: (a) Brij-56 and (b) CTAB as the template.

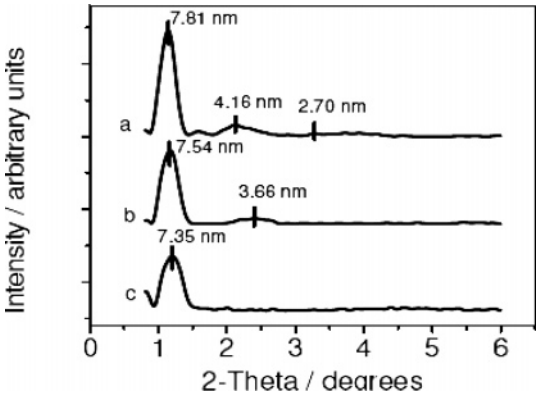

Figure 10. XRD patterns for vinyl-modified particles with different loadings: (a) 7 mol %, (b) 14 mol %, (c) 27 mol %.

(d) Vinyl Functionalization. Figures 8 and 9, respectively, present the XRD patterns and TEM images of particles from a direct vinyl modification. The XRD pattern for particles with Brij-56 as the template in Figure 8a indicates a single peak at a 2θ of 1.39°, which corresponds to a *d* spacing of 6.35 nm. This is in accordance with the wormlike pore structure with a center-to-center distance of 6.40 nm measured in the TEM image (Figure 9a). For the CTAB system, an intense peak at a 2θ of 2.86° representing a *d* spacing of 3.09 nm is observed in the XRD pattern in Figure 8b, and some particles with a hexagonal array of pores are observed during TEM analysis as shown in Figure 9b.

Samples with varying VTMS content have also been prepared and analyzed. As shown in Figure 10a, a sample with 7 mol % VTMS shows an intense peak at a 2θ of 1.13°, which corresponds to a *d* spacing of 7.81 nm, and two weak peaks at 2θ values of 2.12° and 3.27° representing *d* spacings of 4.16 and 2.70 nm, respectively. Lamellar structures are found in TEM observation (Figure 11a,b). By increasing the VTMS loading, the number of diffraction peaks and intensity simultaneously decrease. For example, as shown in Figure 10b,c, two diffraction peaks at 2θ values of 1.14° and 2.41° representing *d* spacings of 7.74 and 3.66 nm are observed for a 14 mol % VTMS sample, while only a single peak at a 2θ of 1.20° representing a *d* spacing of 7.35 nm is found for a 27 mol % VTMS sample. The gradual loss of high-order XRD diffraction and the weakening of the diffraction intensity indicate that further increasing the VTMS concentration may decrease the efficiency of coassembly, leading to a deteriorated long-range ordering. The shifts of *d* spacing from 7.81 to 7.35 nm with the increased VTMS content from 7% to 27% may be due to the incorporation of the vinyl groups into the internal surface of silica particles, which leads to a decreased pore diameter. Vinyl modification results in disordered structures to some extent, but a few particles maintain ordered mesostructures, such as the lamellar structures shown in Figure 11c,d.

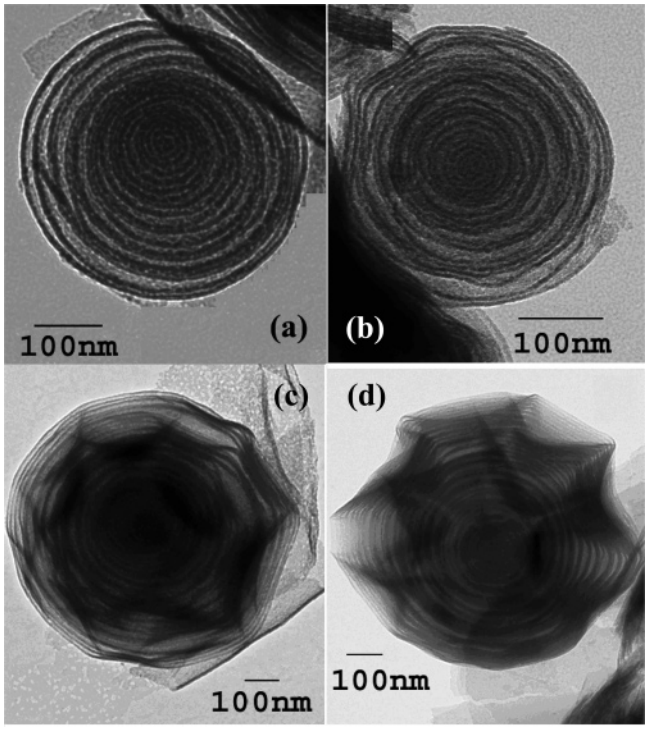

Figure 11. TEM images for vinyl-modified particles with different loadings: (a, b) 7 mol %, (c) 14 mol %, (d) 27 mol %.

(e) TMSPMA Functionalization. The TMSPMA molecule ($CH_2{=}C(CH_3)COO(CH_3)_3Si(OCH_3)_3$) contains a carbon−carbon double bond (C═C) and a methoxylsilane group (Si-$(OCH_3)_3$). The former group is suitable for free radical polymerization, and the latter group can form a three-dimensional silica network through hydrolysis and condensation reactions.[41] Figures 12 and 13 show the XRD patterns and TEM images of TMSPMA-modified silica particles. After TMSPMA modification, the first diffraction peak for all templates shifts to a decreased *d* spacing of 5.55 nm for

(41) Ji, X.; Hampsey, J. E.; Hu, Q.; He, J.; Yang, Z.; Lu, Y. *Chem. Mater.* **2003**, *15*, 3656.

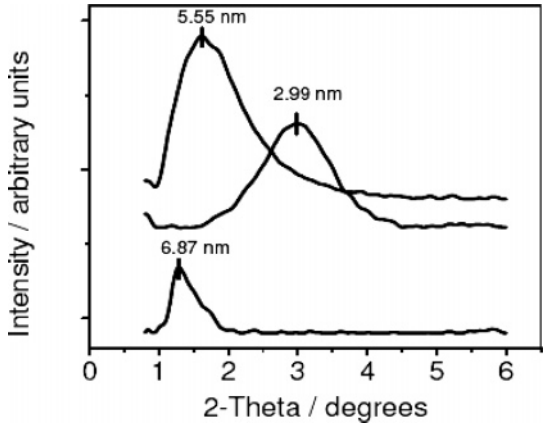

Figure 12. XRD patterns for methyl-modified particles: (a) Brij-56, (b) CTAB, and (c) P123 as the template.

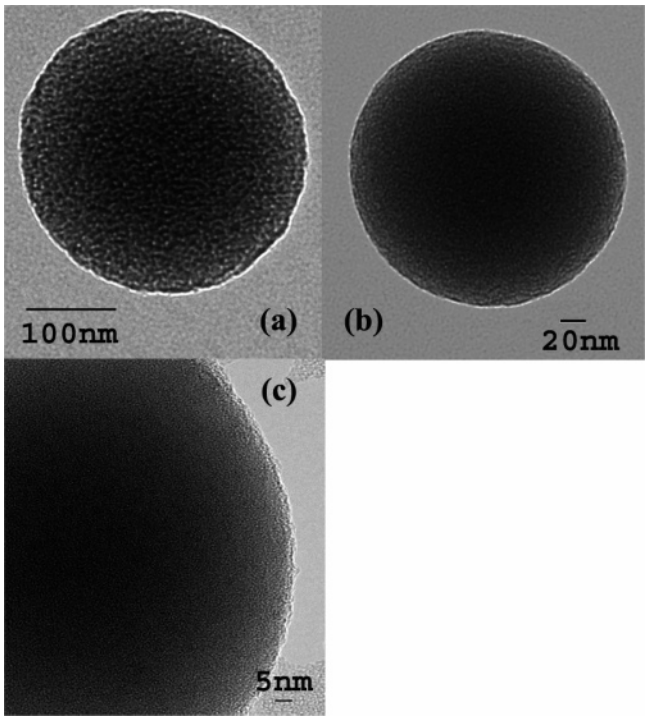

Figure 13. TEM images for TMSPMA-modified particles: (a) Brij-56, (b) CTAB, and (c) P123 as the template.

Brij-56, 2.99 nm for CTAB, and 6.40 nm for P123. As shown in Figure 13, wormlike pore structures can be observed in all the TEM images. The center-to-center distance is approximately 5.60 nm for Brij-56 and 3.07 nm for CTAB.

Figure 14 shows the variation in the *d* spacing for the methyl, vinyl, and propyl methacrylate-modified particles. No matter which surfactants are employed, a longer modifying molecule leads to a smaller *d* spacing (i.e., a smaller pore size due to an attachment of the organic ligands to the silica surface).

FT-IR Spectra. FT-IR spectra (see Figure S1 in the Supporting Information) of the TFTS-modified silica particles before and after heat treatment at 350 °C for 5 h in a nitrogen atmosphere show the strong CH_2 and CH_3 stretching bands (2900 cm^{-1}) of the nontreated sample due to the presence of CTAB and the ethylene group in the tridecafluoro-1,1,2,2-tetrahydrooctyl ligands. Note that tridecafluoro-1,1,2,2-tetrahydrooctyl ligands exhibit strong CF_2 and CF_3 stretching

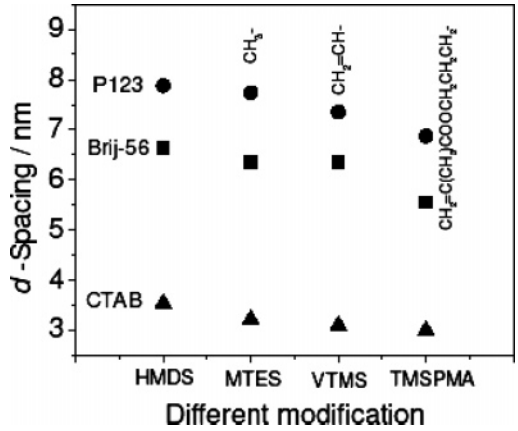

Figure 14. Variation of the *d* spacing with different modifications.

bands at ~1200 and 700 cm^{-1}. Comparing the IR spectra of the samples before and after heat treatment, we see a dramatic decrease in the CH_2 and CH_3 stretching band intensities consistent with the removal of CTAB. However, the spectrum of the heat-treated sample retains the strong CF_2 and CF_3 stretching bands, indicating that tridecafluoro-1,1,2,2-tetrahydrooctyl ligands remain stable in the hybrid materials. The residual CH_2 feature (2900 cm^{-1}) in the heat-treated sample is due to the presence of CH_2CH_2 in the remaining tridecafluoro-1,1,2,2-tetrahydrooctyl ligands. We also observed that heating reduces the intensity of broad absorption bands centered at 3400 cm^{-1} assigned to O−H stretching of hydroxyl groups associated with residual ethanol and uncondensed Si−OH groups. Further condensation of the framework is evidenced by the reduction of the 3400 cm^{-1} band along with a shift of the asymmetric Si−O−Si stretching of the silica network from 1067 to 1073 cm^{-1} and the reduction of the intensity of Si−OH stretching bands around 960 cm^{-1}. The IR spectra confirm that CTAB can be selectively removed by pyrolysis without affecting tridecafluoro-1,1,2,2-tetrahydrooctyl ligands in the hybrid materials. This agrees well with the TGA/DTA results shown in Figure 2.

FT-IR spectra (see Figure S2 in the Supporting Information) of the silica particles using Brij-56 as the template indicate qualitatively that the amount of organosiloxane incorporated into the silica framework is related to the composition of the synthesis mixture. Typically, there are many silanol (SiOH) groups on the surface of mesoporous silica. Pure silica aerosol particles show characteristic bands at 3470 cm^{-1} from the Si−OH stretching vibration and 1640 cm^{-1} assigned to the O−H stretching vibration (overtone) and bands at 1090, 974, 806, and 471 cm^{-1} due to the Si−O stretching vibration. A very intense and broad band at a high-frequency region between 3700 and 3200 cm^{-1} implies the presence of hydrogen bonding in the mesoporous silica. The band due to the asymmetric Si−O−Si stretching vibration is located at 1090 cm^{-1} with a much more intense and broad band. The appearance of an additional peak at 2960 cm^{-1} in the silica particles posttreated with HMDS indicates the CH_3 asymmetric stretching vibration. The three peaks at 1270, 849, and 765 cm^{-1} are associated with both methyl vibrations and the Si−C stretching vibration. For the methyl-modified silica sample, bands related to methyl groups occur at 2965

Table 2. Chemical Shifts, Corresponding Relative Peak Areas Obtained by Curve Deconvolution, Degree of Silica Condensation, and Percentage of Organic Incorporation of Modified Mesoporous Silica Particles Obtained from ^{29}Si MAS NMR (P123 as the Template)[a]

	δ (ppm) [relative peak area]				degree of condensation	organic incorporation (%)
	T^2	T^3	Q^3	Q^4		
calcined			−102.3 [75.8]	−111.1 [24.2]	81.0	
HMDS			−103.0 [45.0]	−111.3 [55.0]	88.8	
M1 (22 mol % MTES)		−64.8 [25.0]	−102.1 [28.5]	−110.2 [46.5]	92.9	25
V3 (7 mol % VTMS)	−64.7 [3.6]	−81.5 [5.4]	−102.9 [48.4]	−110.8 [42.6]	87.0	9
V2 (14 mol % VTMS)	−71.2 [1.1]	−80.9 [11.0]	−102.5 [36.4]	−110.5 [51.5]	90.6	12
V1 (27 mol % VTMS)	−72.9 [4.8]	−80.7 [23.4]	−101.8 [33.3]	−110.0 [38.5]	90.5	28
T1 (30 mol % TMSPMA)	−59.6 [7.8]	−67.2 [22.0]	−102.0 [34.1]	−110.4 [36.1]	89.5	30

[a] Q^3 and Q^4 represent silicon atoms (denoted as Si*) in $HOSi^*(OSi)_3$ and $Si^*(OSi)_4$ silicate species, respectively. T^2 and T^3, respectively, represent the silicon atoms (denoted as Si*) in $RSi^*(OH)(OSi)_2$ and $RSi^*(OSi)_3$ species, where R is the nonhydrolyzable ligand.

and 1270 cm^{-1} with a sharp peak at 765 cm^{-1}. A peak at 1640 cm^{-1} possibly comes from the O−H stretching vibration (overtone). Vinyl-modified silica exhibits a weak peak at 1610 cm^{-1} arising from the C═C stretching vibration, a weak peak at 1410 cm^{-1} related to the CH_2 in-plane deformation vibration, and a sharp peak at 968 cm^{-1} associated with the CH_2 wagging vibration. The C−H stretching vibration is observed at 2970 cm^{-1}. Interestingly, the band between 3700 and 3200 cm^{-1} due to hydrogen bonding almost virtually disappears after vinyl functionalization, which is well understood with respect to the hydrophobic surface in the mesopores. For the TMSPMA-modified sample, the C−H stretching vibration appears at 2960 cm^{-1} while the band at 1742 cm^{-1} is assigned to the C═O stretching vibration. Bands associated with the C═C vibration have been observed at 1670 and 935 cm^{-1}, along with a band at 1445 cm^{-1} possibly from the O−CH_2 and CH_3 vibrations. A band appears at 1260 cm^{-1} due to the C−O−C asymmetric stretching vibration. The organosiloxane peaks are still present in the IR spectra for samples with removed surfactants, confirming that the organic moieties are linked covalently to the mesoporous silica framework. Similar results have been observed in the CTAB and P123 systems.[12,15,42−45]

Solid-State NMR Spectroscopy. *(a) Solid-State ^{13}C CP-MAS NMR Spectroscopy.* The presence of the organic functional groups within the mesoporous particles was also confirmed by solid-state ^{13}C CP-MAS NMR. In Figure S3 (Supporting Information), a sample posttreated with HMDS exhibits a signal at 16.7 ppm due to methyl groups and one at −0.1 ppm due to CH_2 groups. A peak at approximately 59.0 ppm appears in all samples and is possibly related to residual ethanol solvent. MTES-modified silica particles display a resonance at −4.4 ppm due to CH_3Si groups. For vinyl-modified silica aerosol particles, characteristic resonances appear at 137.5 and 128.6 ppm for carbon−carbon double bonds. By increasing the VTMS loading, only a slight shift is observed. TMSPMA-modified particles exhibit resonances of the vinyl carbons at 122.9 and 136.7 ppm, the methyl group (CH_3) attached to the vinyl group (C═C) at 22.0 ppm, and the ester carbon group (−OCH_3) at 166.0 ppm. The resonances at 66.0, 17.7, and 0.9 ppm are related to the propyl groups. A resonance at 8.4 ppm possibly comes from the carbon in the $Si(OCH_3)$ groups, indicating an incomplete hydrolysis of the TMSPMA molecules. A resonance at 59.0 ppm is perhaps due to residual ethanol solvent. These data further confirm the organic functionalization of the mesoporous silica particles.

(b) Solid-State ^{29}Si MAS NMR Spectroscopy. ^{29}Si NMR spectroscopy was used to evaluate the degree of condensation (the relative number of siloxane bonds to each silicon atom) and the degree of organic incorporation into the networks ([T]/([T] + [Q])). Q^3 and Q^4 represent silicon atoms (denoted as Si*) in $HOSi^*(OSi)_3$ and $Si^*(OSi)_4$ silicate species, respectively. T^2 and T^3, respectively, represent the silicon atoms (denoted as Si*) in $RSi^*(OH)(OSi)_2$ and $RSi^*(OSi)_3$ species, where R is the nonhydrolyzable ligand.

A peak at −110 to −111 ppm comes from Q^4, the peak at −102 to −103 ppm corresponds to Q^3, and the other peaks are related to T^2 and T^3 (see Figure S4 in the Supporting Information). Table 2 summarizes the chemical shifts, their deconvoluted peak areas, and the degree of condensation. Both calcined samples and samples posttreated with HMDS show only Q^3 and Q^4 resonances. The presence of the T units (T^2 + T^3) further suggests the incorporation of organic ligands within the mesoporous silica particles. For methyl-modified silica particles, the T^3 signal appears at −64.8 ppm. Compared to the starting composition of 22 mol % MTES, 25 mol % organic incorporation was found. Except for the calcined sample, other silica particles exhibit a degree of condensation of about 90%. In Table 2, the molar percentage of the T units measured in NMR is close to the molar percentage of the modified agents used in the synthesis process.

Nitrogen Adsorption−Desorption. Generally, highly ordered surface-modified mesoporous silica is difficult to obtain using organotrialkoxysilanes because the structure of the surfactant micelle is perturbed by the organic groups that share the same confined channels. Nitrogen adsorption studies confirm that all the functionalized silica aerosol samples except the CTAB system are mesoporous and similar to pure silica particles (Figure 15). They all show type IV isotherms, which is characteristic of mesoporous materials according to the IUPAC classification. However, unlike the sample prepared with pure TEOS which exhibits a type IV isotherm, the samples prepared from MTES, VTMS, TMSPMA, and TEOS using CTAB as the structure-directing

(42) Sellinger, A.; Weiss, P. M.; Nguyen, A.; Lu, Y.; Assink, R. A.; Gong, W.; Brinker, C. J. *Nature* **1998**, *394*, 256.
(43) Lebeau, B.; Fowler, C. E.; Hall, S. R.; Mann, S. *J. Mater. Chem.* **1999**, *9*, 2279.
(44) Christiansen, S. C.; Zhao, D.; Janicke, M. T.; Landry, C. C.; Stucky, G. D.; Chmelka, B. F. *J. Am. Chem. Soc.* **2001**, *123*, 4519.
(45) Huang, L.; Wang, Z.; Sun, J.; Miao, L.; Li, Q.; Yan, Y.; Zhao, D. *J. Am. Chem. Soc.* **2000**, *122*, 3530.

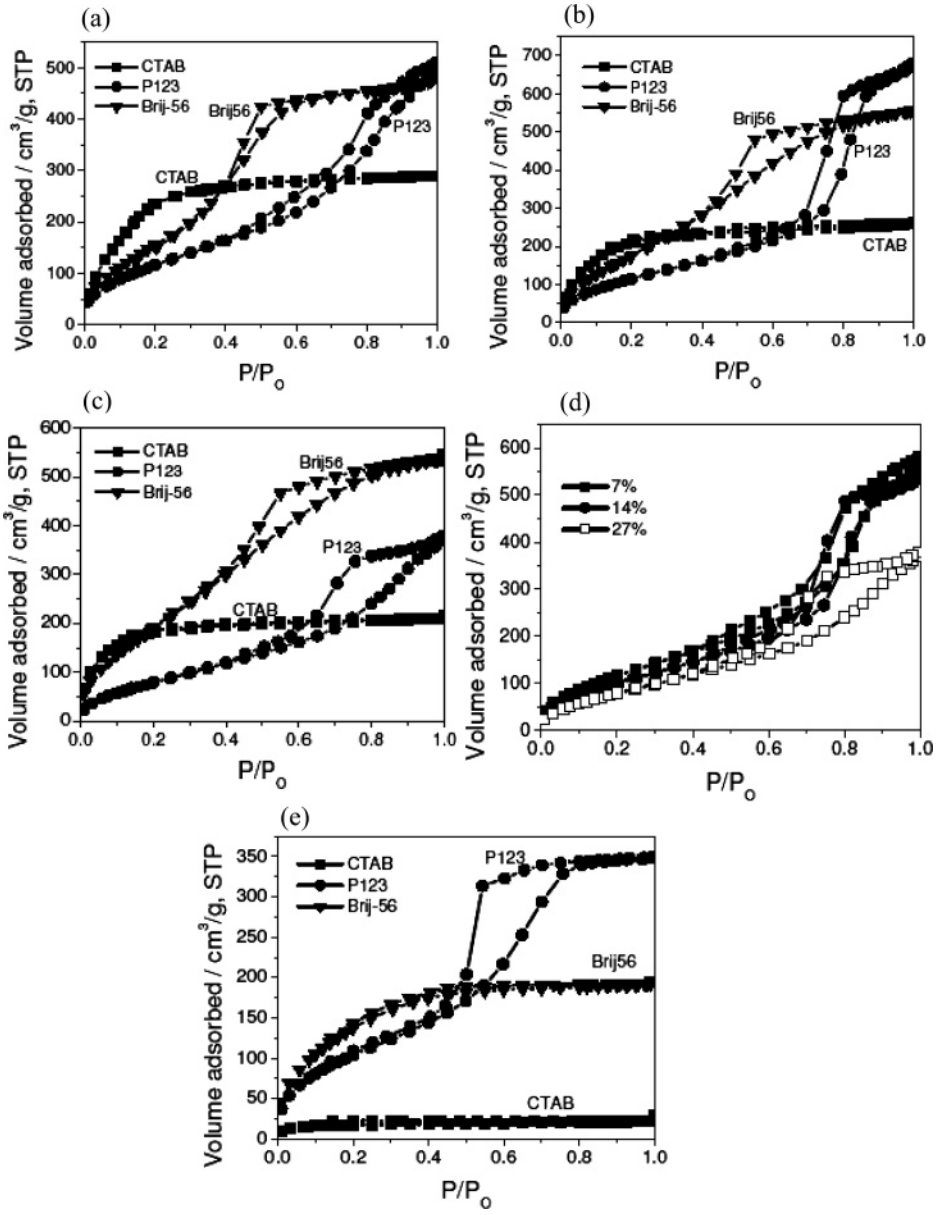

Figure 15. Nitrogen adsorption−desorption isotherms for silica particles functionalized with (a) HMDS, (b) MTES, (c) VTMS, (d) different VTMS loadings using P123 as the template, and (e) TMSPMA.

agent present a type I isotherm, typical of microporous solids. For example, the adsorbed volumes, no matter what kind of functionalization, exhibit a very low and saturated value at a relative pressure (p/p_o) below 0.2, indicating the pressure characteristic of micropores. Therefore, no peak occurs in the pore size distribution curves in Figure 16a−c,e. Furthermore, reversible isotherms are observed only for the above system. All other samples show slight or large hysteresis loops. For example, Brij-56-assembled silica samples posttreated with HMDS exhibit a large hysteresis loop at p/p_o between 0.4 and 0.6, while the corresponding P123 sample shows a very large hysteresis loop starting from $p/p_o = 0.4$ in Figure 15a.

Methyl-functionalized silica samples display different isotherms in Figure 15b. The Brij-56 sample shows a large hysteresis loop in the p/p_o range of 0.4−0.8. A similar hysteresis loop has been observed in the P123 sample from $p/p_o = 0.4$ to $p/p_o = 1.0$. For vinyl-functionalized samples, a larger hysteresis loop is seen in Figure 15c for both the Brij-56 and P123 systems, which starts at $p/p_o = 0.4$ and extends to $p/p_o = 1.0$. Increasing the VTMS percent content leads to a larger hysteresis loop as shown in Figure 15d. Different isotherms are shown for TMSPMA-modified samples in Figure 15e. Only the P123-assmbled silica shows a large hysteresis loop between $p/p_o = 0.4$ and $p/p_o = 0.8$.

The specific surface areas of all samples are calculated by the BET method, and the pore sizes are obtained from the BJH model. The BET results are listed in Table 3. The related pore size distribution curves are shown in Figure 15. CTAB always provides smaller pore diameters than other surfactants such as Brij-56 and P123. The BET surface areas of mesoporous silica posttreated with HMDS are 1038 (CTAB), 644 (Brij-56), and 456 (P123) m^2/g, and the pore volumes are 0.45 (CTAB), 0.73 (Brij-56), and 0.75 (P123) cm^3/g. The Brij-56 silica sample possesses a broad pore size distribution while the P123 sample exhibits a very wide pore size distribution as shown in Figure 16a. Methyl-functionalized silica samples show surface areas of 836 (CTAB),

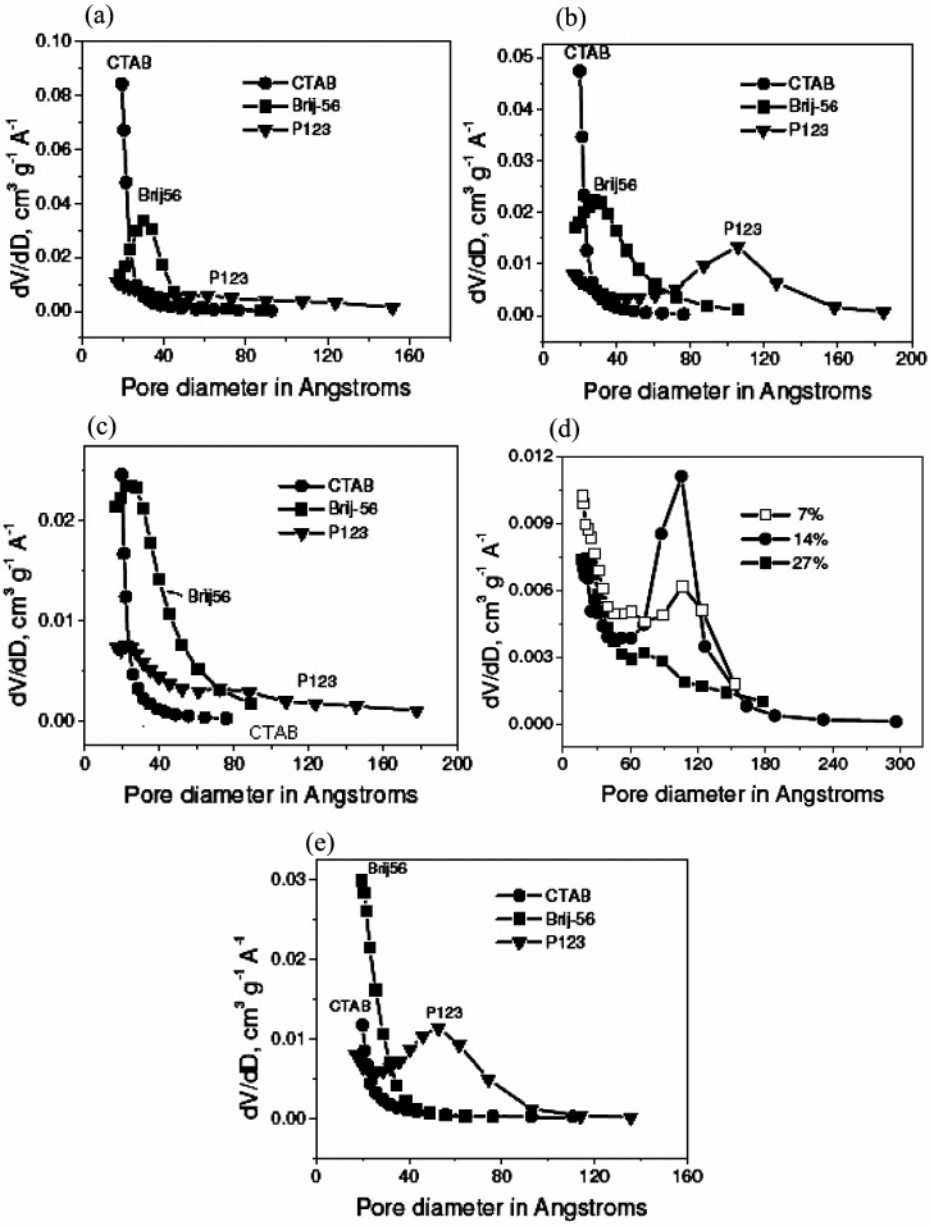

Figure 16. Pore size distributions for particles modified with (a) HMDS, (b) MTES, (c) VTMS, (d) different VTMS loadings using P123 as the template, and (e) TMSPMA.

Table 3. Surface Areas, Pore Diameters, and Pore Volumes of Organic Functionalized Mesoporous Silica

surfactant	composition (mol %)	surface area[a] (m^2/g)	pore vol[b] (cm^3/g)	av pore diam[c] (Å)
CTAB	100% TEOS followed by HMDS treatment	1038	0.45	
CTAB	22% MTES + 78% TEOS	836	0.40	
CTAB	27% VTMS + 73% TEOS	675	0.32	
CTAB	30% TMSPMA + 70% TEOS	593	0.31	
Brij-56	100% TEOS followed by HMDS treatment	644	0.73	45.5
Brij-56	22% MTES + 78% TEOS	724	0.85	36.8
Brij-56	27% VTMS + 73% TEOS	783	0.83	34.4
Brij-56	30% TMSPMA + 70% TEOS	577	0.38	29.3
P123	100% TEOS followed by HMDS treatment	456	0.75	58.6
P123	22% MTES + 78% TEOS	456	1.02	73.4
P123	27% VTMS + 73% TEOS	321	0.55	59.1
P123	14% VTMS + 86% TEOS	404	0.81	66.9
P123	7% VTMS + 93% TEOS	468	0.86	64.7
P123	30% TMSPMA + 70% TEOS	407	0.54	44.0

[a] BET surface area. [b] Single-point pore volume. [c] BJH average pore diameter.

724 (Brij-56), and 456 (P123) m^2/g, pore volumes of 0.40 (CTAB), 0.85 (Brij-56), and 1.02 (P123) cm^3/g, and relative average pore sizes of 36.8 (Brij-56) and 73.4 (P123) Å. Vinyl-modified samples show surface areas of 675 (CTAB), 783 (Brij-56), and 321 (P123) m^2/g, pore volumes of 0.32 (CTAB), 0.83 (Brij-56), and 0.55 (P123) cm^3/g, and average pore diameters of 34.4 (Brij-56) and 59.1 (P123) Å. The BET specific surface areas and pore volume of these modified silicas decrease with increasing amounts of functionalized organosilane. For example, in the VTMS/silica/P123 samples, the 7% VTMS sample has a surface area of 468 m^2/g, a pore volume of 0.86 cm^3/g, and a BJH average pore size of 64.7 Å, while the 27% VTMS sample has a surface area of 321 m^2/g, a pore volume of 0.55 cm^3/g, and an average pore size of 59.1 Å. The decreased pore size is in good agreement with the decreased *d* spacing observed from XRD measurements. The pore size distribution tends to be wider with increasing VTMS content as illustrated in Figure 16d. The above result is in accordance with the large hysteresis loop shown in Figure 15d. Furthermore, the micropores occupy

some volume determined from the pore size distribution curve in Figure 16d. In particular, TMSPMA-functionalized samples using Brij-56 and P123 as structure-directing agents exhibit a large decrease in pore diameter, such as 26.7 Å for Brij-56 and 44.0 Å for P123.

From the above discussion, it can be concluded that an increase of the organosilane content leads to decreases in the pore size, pore volume, and surface area. There are two possible reasons for this phenomenon. Since each organosilane molecule used in our experiments, for example, TFTS, MTES, VTMS, and TMSPMA, contains only three reactive ethoxy groups compared with four groups in a TEOS molecule, an increased organosilane concentration may weaken the silicate framework modulus and promote collapse or shrinkage of the silicate framework upon the removal of the surfactant templates. This in turn produces mesoporous materials with smaller pore sizes and less ordered pore structure. Also, the presence of the organic groups on the pore surface may have contributed to the decreased pore sizes and pore volume.

Conclusions

On the basis of aerosol-assisted self-assembly, functionalized mesoporous silica materials have been prepared via a direct co-condensation of TEOS and organosilanes. XRD patterns and TEM images indicate ordered and disordered structures such as hexagonal, lamellar, or wormlike structures after surface modification. FT-IR and NMR spectra confirm that organic moieties, such as fluoro, methyl, vinyl, and propyl methacrylate, are linked covalently to the internal surface of the mesoporous channels. The molar percentage of the organic incorporation measured from NMR is close to the molar percentage of modified agents used in the synthesis process. Most functionalized samples are mesoporous and possess a decreased surface area, pore volume, and average pore size due to an attachment of organic ligands to the surface of the silica particles. Increasing the chain length of the organic ligands results in a decrease in the *d* spacing of the first diffraction peak of the XRD patterns, which is also in accordance with the BET results. This aerosol process is an efficient, productive, and low-cost method to produce organically modified mesoporous silica particles via a direct co-condensation synthesis. This method provides a productive route to produce mesoporous silica particles with various organic ligands for catalyst, filler, and other applications.

Acknowledgment. We thank Dr. T. Ji and Dr. J. Fang for their assistance in the FT-IR measurement and Mr. Pierre Burnside for assistance in the XRD measurement. This work is financially supported by NASA (Grant No. NAG-1-02070 and NCC-3-946), Office of Naval Research, Louisiana Board of Regents (Grant No. LEQSF (2001-04)-RD-B-09) and National Science Foundation (Grant No. NSF-DMR-0124765 and CAREER award), and the Advanced Materials Research Institute at the University of New Orleans through DARPA Grant No. MDA972-97-1-0003 and through the Louisiana Board of Regents Contract No. NSF/LEQSF (2001-04)-RII-03.

Supporting Information Available: Five additional figures (PDF). This material is available free of charge via the Internet at http://pubs.acs.org.

CM052764P